)

RESULTS OF LONG TIME PHOTOMETRIC AND SPECTRAL OBSERVATIONS OF HERBIG BE STAR AS 310

N. Z. Ismailov [a*], *V. Bakış* [c**], *S. A. Alishov* [a], *Sh. K. Ismayilova* [a],

F. S. Huseynova [b]

[a] *N.Tusi Shamakhy Astrophysical Observatory of Azerbaijan National Academy of Sciences, Shamakhy, Azerbaijan*

[b] *Batabat Astrophysical Observatory, Nakhichevan, Azerbaijan*

[c] *Department of Space Sciences and Technologies, Faculty of Sciences, Akdeniz University, Antalya, Türkiye.*

The results of spectral and photometric studies of Herbig's Be-type star AS 310 have been presented. Photometric observations in the BVRcIc bands performed in 2016–2021 showed that the amplitude of the seasonal brightness variations of the star changes smoothly in different years and reaches a maximum of $\Delta V \sim 0.6$ mag in 2018. The star is more often in a weak state brightness, but from time to time, there is an increase in brightness. With a decrease in brightness in the V-band, the star's radiation in the blue color increases, while it weakens in the red part of the spectrum. Searches for periodic brightness changes have not revealed significant periods of variability. The emission components observed in the hydrogen lines are rather formed in the nebula where the star itself is immersed. The spectrum contains strong lines of neutral helium, without any signs of emission components. The spectral class corresponds to the combined spectrum B3-5V + B1.5-2V. Our studies have shown that AS 310 is an extremely young binary star that has lost its circumstellar protoplanetary disk.

Key words: Pre-Main sequence stars – HBe stars – young stellar clusters – photometry – spectroscopy – variability

1. INTRODUCTION

To date, the formation and early evolution of massive stars have been studied very poorly. Immediately after birth, such stars are surrounded by dark gas and dust disks, which causes enormous optical absorption. The existence of the strong stellar wind further complicates the picture. It is expected that the time to enter the MS for massive young stars should be relatively short, so the processes of dissipation of the circumstellar disk and the formation of planets should be qualitatively different from those for cold low-mass stars. It is also unknown at what stage massive young stars lose all the characteristic properties of the HAeBe star phenomenon and turn into ordinary OB stars.

Herbig Be type stars (HBe) is a subclass of young intermediate-mass stars, the so-called Herbig AeBe-type stars (HAeBe), (Herbig 1960). For classical HBe stars, the upper mass limit was considered by many authors to be 8-12 $M_\odot$ (see, for example, Herbig, 1960, Finkenzeller & Mundt 1984). Using Gaia Observational Data DR 3 (Verhoeff et al., 2020, Guzman - Diez et al. 2021) showed that for HBe stars the maximum expected mass could be more than 20 $M_\odot$. There are only several studies on the individual characteristics of massive HBe stars (see, for example, Pogodin et al .2017, Ismailov et al.2020a). Studying the characteristics of massive HBe stars is an important task for understanding the evolution of such stars. This paper presents the results of studies of the HBe star AS 310.

The catalogue (Herbig&Bell, 1988) lists the star HBC 284 = AS 310 as a hot, high-luminosity HAeBe star, which is notable for significant signatures of strong interstellar absorption bands in the spectrum. The spectrograms show an intense Hα emission line and narrow helium absorption lines. According to Georgelin&Georgelin (1970), the star is in the HII (S 61) region. Finkenzeller & Mundt (1984) note that the star does not show a broad emission in the Hα line, so the object cannot be considered a Herbig star. The star at position 135° at an angular distance of 3″ has a companion with a brightness difference Δm ≈ 1mag. Based on observations in the region of 1.3 mm Henning et al. (1994) showed that the mass of the source is estimated at about 30M⊙.

According to Bastian & Mundt (1979), the star AS 310 has a close companion at an angular distance of 4",and both stars contribute to the radiation. Brooke et al. (1993) based on observations in the range of 3μm give the spectral type of the star as B2 + B5. According to their data, the energy distribution in the spectrum (SED) satisfactorily agrees with the model of a star with a temperature of 20000 K. According to these authors, it is possible that the stars numbered 1 and 2 given in Lahulla (1987) in the H61 region belong to these components. However, Hunter & Massey (1990) report a spectral type of B1I, and a high degree of interstellar extinction. We have collected data from different authors in

Table 1.

As can be seen from Table 1, some parameters of the star differ significantly for different authors. The main reason for this difference seems to be the complex circumstellar environment and the inaccuracy in determining the interstellar reddening coefficient.

AS 310 is at a distance of 2500 pc (Ageorges et al., 1997; Testi et al., 1998) and shows a lot of gas and dust in the region (Hernandez et al., 2004). It has been shown that stellar components are located at an angular distance of a few arcseconds from the central source, and bipolar jets are also observed (Goodrich, 1993).

Thus, to understand the mechanism of star formation in massive young stars associated with HAeBe stars, more observational studies of systems like AS310 are paramount.

2. PHOTOMETRIC OBSERVATIONS.

Our photometric observations of the star were carried out on the Zeiss -600 telescope by using a BVRcIs photometer, which is mounted in the Cassegrain focus of the telescope (F = 7500 mm) with a relative aperture $A = 1 : 12.5$. As a light detector has used CCD FLI 4Kx4 K camera with the size of the element 9μm. The useful field of the image frames was 17'x17'. When applying binning 2×2 or 4×4, the resolution per pixel has obtained 0.49"/px or 0.99"/px. The photometric data were obtained and processed using the standard procedures of the MaximDL, software package. A detailed description of the photometric system is given in (Abdullayex et al. 2012). Transformation of our photometric system to the international one was carried out in the work (Valiyex et al. 2022).

Under the astroclimate of ShAQ, the turbulent circle of the star is mainly 1.5-2". Under such conditions, the components located at an angular distance of 3-4", which were noted in the works (Finkenzeller & Mundt, 1984, Bastian & Mundt, 1979) with a 4x4 binning combination will not be resolved. In the obtained fits-format frames, the star image did not differ in shape from a circle, and when the brightness was measured, the image of the object was completely covered by the chosen aperture size of the measuring circle. In this case, the aperture size of the measuring circle was about 6". The average root-mean-square measurement error according to our data in individual bands was ± 0.02 B, ± 0.008 V, ± 0.005Rc, ± 0.009Ic.

Our photometric observations cover the period 2016-2022. A total of 82 measurements were obtained in the V band, slightly less in the other bands. A table with the results of our photometric observations was published by Valiev et al. (2022).

Table 1. Some parameters of the star, which were collected from the literature.

References	Teff, K	Log g $\left[\, \text{cm} + \text{s}^{-2}\right]$	D, pc	Av	Log L/LQ	R, R⊙	M, M⊙	age, Myr	Sp	EW Hα
Wichittanakom et al. 2020	26000	4.4	2110	3.86	4.13	5.7	11.6	0.07± 0.08	B1e	
Verhoeff et al. 2012	25100		2500	3.7	4.23	6.8	12		B1e	
Xirque et al. 2020	24500		2110	4,13	4.17		11.9	0.06		-8.89
Testi et al. 1998	30900		2500		4.55				B0	
Brooke et al. 1993			2500	3.9					B2+B5	
Manoj et al. 2006	25100		2500	6.06	5.21		> 6.00	< 0.01	B1	-7.7 -5.0
Hernandez et al. 2004	25100		2500	4.1, 6.6	4.43 5.43		14.5, 43.5	0.02 0.01	B1, B0, BA	-7.7
Guzman_Diaz et al. 2021	28000		2380	4.0	4.34	6.32	14.4	0.05	B0	
Henning et al. 1994	30900		2500		3.0		30		B0	

Figure 1 shows the star's light curve obtained on our B and V bands data. The vertical line segments indicate the dates on which our spectral observations were made. As can be seen, the star is mostly in a weak state of brightness, but at times it shows an increase in brightness with different amplitudes during the observation season. Over 6 years of observations of the star, the amplitude of brightness changes in the V band gradually increases and reaches a maximum of about 0.6 mag in 2018. Further, until 2022, a gradual decrease in the amplitude of brightness changes is observed. The brightness variability in the B band has the same character as in the V band. Unfortunately, on the night of observations of the maximum amplitude in the V band, observations in the B band were not made, so the change in the amplitude on the same night in the B band could not be observed.

In Figure 2 is shown the color-index diagrams, where variations of B-V, V-Rc, and V- Ic colors of the star as a function of V-band brightness are presented. As can be seen, as the brightness decreases, the B-V color index increases, in other words, the star's radiation is enhanced in the blue, and the color indices V- Rc and
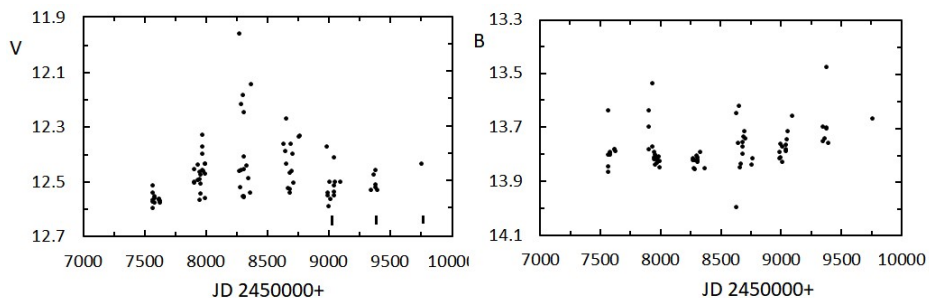
Fig. 1. Variation in the brightness of the star in the V (left panel) and B -bands (right panel), obtained from our data for 2016-2022. On the left panel, the dates of our spectral observations are indicated by vertical line segments.

V- Ic have shown decreasing, i.e., the radiation in the red part of the spectrum is weakened. Such a change indicates that the brightness variability can be caused by the enhancement of radiation in the violet part of the spectrum.
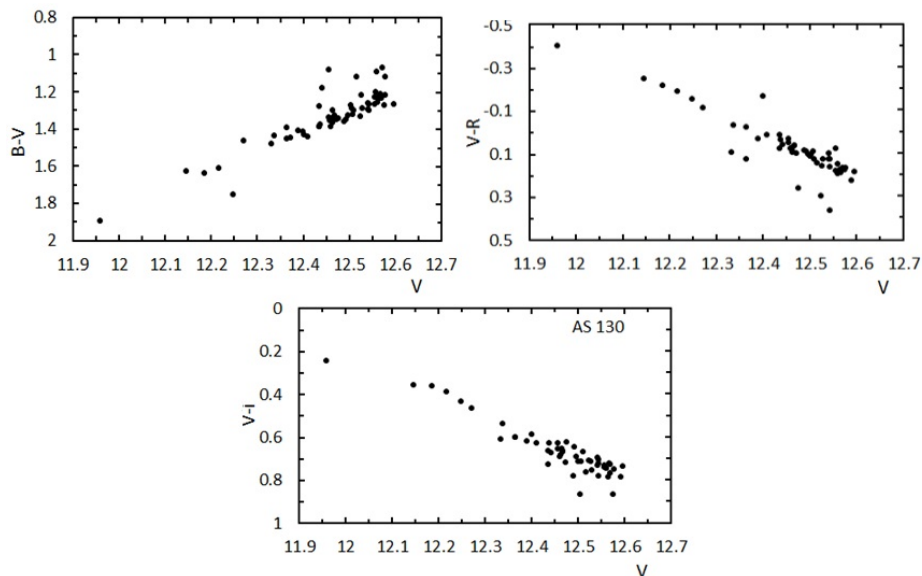

Fig. 2. Variations of the color indexes B-V, V-R and V-Ic versus V-band brightness.

3. SEARCHING FOR A PERIODICAL VARIATION IN THE BRIGHTNESS

To search for periodic components in the brightness variations of the star, we used the Fourier analysis, which used the method of Lomb (1976) and Cargle (1982). The search was performed by the Period 04 program (Lenz & Breger, 2005). The program is designed for statistical analysis of large astronomical time series containing gaps in time. The program offers tools for extracting individual frequencies from multi-period time series content and provides a flexible interface for performing multiple frequency fitting.

The source material for performing the Fourier analysis was the observational data obtained from the archive (Herbst and Shevchenko, 1999). Photometric UBVR measurements of the star have been carried out for 6 years since 1983 at the Maidanak Observatory of the Institute of Astronomy of Uzbekistan. Data from this archive are given in Herbst and Shevchenko (1999) and Grankin et al. (2007). Only 344 measurements were taken from this archive in the V band, some less in the UBR bands. This material was supplemented by 82 measurements in the V band obtained by us. There are no systematic differences between our data and catalogue data. The collected photometric material was divided into separate
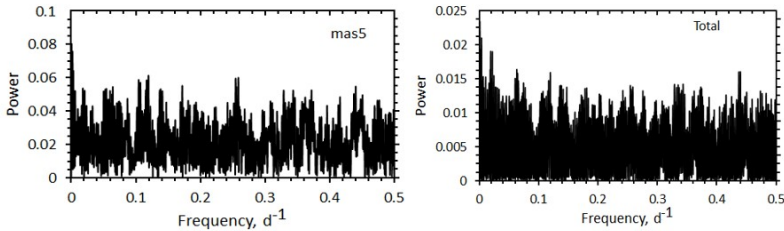

Fig. 3. Examples of the power spectrum for the array with 77 points obtained in 1990 (left) and for all observations simultaneously (right).

files according to the years of observations and was also cleared of trends indicating long-term changes in the average brightness. In total, 6 different arrays were considered, each of which has more than 60 points. For each of the arrays of points, the period was searched separately. In none of the considered arrays, an explicitly allocated value of the period was found. Figure 3 shows, as an example, the power spectrum for an array covering the interval of observations for JD 244 8049-244 8163 (1990) for 77 points of the array. The right panel of Fig. 3 shows the power spectrum for all observational data. As can be seen, a certain period in the change in the star's brightness is not clearly distinguished in the power spectra.

4. SPECTRAL OBSERVATIONS

Spectral observations of the star AS 310 have been made at the ShAO 2-m telescope Cassegrain focus by using the UAGS spectrograph (Universal Astro Grid Spectrograph). As a light detector Andor CCD camera (ikonL-936-BEX2-DD), which is working with a matrix of 2048×2048 elements has been used, pixel size $1\text{px} = 13.5\mu\text{m}$. To adapt the CCD to the spectrograph, in the camera of the spectrograph, a fast lens Canon EF ($f = 200$ mm, $f/2$) was used. The focal length of the collimator f coll $= 1100$ mm, cameras $f_{cam} = 200$ mm, angle of incidence α and diffraction angle β are $27.5°$ and $20.5°$, respectively. The resolution in the camera focal plane is determined by the width of two pixels, so for binning 1×1 the monochromatic image of the slit is $S' = 2\text{px} = 0.027$ mm. Then for the spectrograph's entrance slit width, we obtain $S = 0.145$ mm. The focal length of the Cassegrain focus of a 2 m telescope is F $= 29500$ mm, and the focal plane scale is $\mu = 6.99$"/mm. Then for the width of the entrance slit, we have to get $0.99''$. Similarly, for binning 2×2, we have got a size of $1.99''$. In this complex the spectra of standard stars, various types of variable stars and galaxies were obtained. Moreover, for the Gaia program, the spectra of various transient objects were obtained (see, for example, Ismailox et al. 2020b, Gezer et al. 2020).

A diffraction grating of 651 lines /mm was used, which at a diffraction angle of $20.5°$ in the first order and at binning 1x1 gives the spectrum with a linear inverse dispersion of 144/mm in the range of $\lambda\ 3600 - 8000$. With the combination of binning 1×1, the spectrum is obtained with an inverse linear dispersion D $= 1.9$/px. In other words, in the region of the Hα line ($\lambda 6562.816$) in this mode, we have obtained a moderate spectral resolution of about $R = 3400$. A more detailed description of the spectrograph and the observation method is given in Ismailov et al.(2023).

For calibration, auxiliary files flat, bias, dark, as well as the calibration spectrum of the lamp ThAr were obtained. Andor CCD Camera for observations managed by Program Solis 4.31 allows changing various parameters during observations, such as binning, exposure time, operating mode, etc. The obtained spectra were further processed using the DECH 20 program and its modifications (Galazutdinox G., http://www gazinur.com/DECH-software.html). All processing was performed by the standard method. Measurements of radial velocities for standard stars in different lines of the spectrum with binning 1×1, depending on the signal-to-noise ratio, is $\pm 3 - 10$ km/s. The equivalent widths of the strongest hydrogen lines in A0-A6 stars can be determined with an error of $\pm 0.5 - 1.0$ Å.

5. GENERAL CHARACTERISTICS OF AS 310 SPECTRUM

The spectra of the star AS 310 were obtained in 2020-2022. As can be seen from Fig.1, our spectral observations were obtained in seasons when the brightness amplitude variations in the V band gradually is decreasing. Fig. 4 shows a general view of the spectrum and the two most interesting regions of the star's spectrum for different dates. The Hα line is observed in the form of a strong emission, which is barely distinguished from the emission doublet of the forbidden line [NII] λ6548 and 6584 on the left and on the right. The full width at half maximums (FWHM) of both the H α line and the forbidden lines are about 8 ± 1.5 and practically do not show large variations. The H β line has a relatively weak emission component, the intensity of which varies significantly on different dates until it completely disappears. The FWHM of the emission component in the H β line is well measured at JD 2458995 , for which we obtained a value of 7.6 ± 1.2. As can be seen, the strongest emission components in these lines practically have the same FWHM. As shown by Ismailox et al. (2023), the instrumental contour for the UAGS spectrograph with binning 1x1 is about 4.5. Consequently, for the expansion of the emission lines under consideration, we obtain only about ~ 180 km/s. This result suggests that all the above-mentioned emission components of various lines are formed in the HII region dark reflection nebula, where the star AS 310 itself is immersed. The remaining lines of the Balmer series are observed in the form of absorption and contain weak emission in the core. The spectrum of the star also contains emission lines of the [OI] λ6300 and 6363 doublet (Fig.4c). In addition, the spectrum of the star shows interstellar absorption lines (DIBs), as well as some Fe II absorption lines (Fig. 5).

The Hβ line has a relatively weak emission component, the intensity of which varies significantly on different dates until it completely disappears. The remaining lines of the Balmer series are observed in the form of absorption. The spectrum of the star also contains emission lines of the [OI] λ.6300 and 6363 doublet (Fig. 4c). In addition, the spectrum of the star shows lines of interstellar extinction (DIBs), as well as some lines of Fe II (Fig. 5). For comparison, the spectrum of the star in the range $\lambda 4000 - 5000$ for four observation dates is shown in Fig. 5. As can be seen from Fig.5, on the night of JD 2458995 there is a strong emission peak in the Hβ and on a weak form in Hγ, lines. In the spectrum obtained 4 days later, on the night of JD 2458999 , the intensity of the emission in these lines decreased significantly.

Figure 6 shows graphs of changes in the equivalent widths and half-widths of these lines in time. It can be seen from the graphs in Fig. 6 that on the first two dates of observations, the EW values for the hydrogen lines are much larger than for the rest of the observation dates.

Fig. 4. Full view of the normalized spectrum of AS 310 (a), as well as parts of the spectrum in the interval λ3900-4900 Å(b) and λ 5600-6700 Å(c).

Fig. 5. Spectra of the star AS 310 in the interval λ4000-5000 Åobtained on different nights.

As can be seen from Fig. 6, the values of the equivalent widths of the $H\alpha$ emission lines according to the spectra obtained in 2020 are greater than in other

Table 2. Equivalent widths of selected helium absorption lines.

	EW(Å),HeI						
JD2450000+	4026	4387	4438	4471	4921	5876	6678
8995.291	0.79	1.39	2.41	1.58	0.79	1.44	2.58
8999.421	1.02	2.36	2.84	1.91	1.62	2.79	2.83
9054.321	0.94	1.78	2.17	1.57	1.19	2.81	1.38
9471.301	0.88	0.69	1.96	1.53	0.89	2.62	1.70
9733.419	0.84	0.78	1.55	1.07	0.83	1.74	1.13
9752.353	0.96	0.79	1.02	1.01	0.65	1.03	0.88
mean	0.91	1.30	1.99	1.45	1.00	2.07	1.75
RMS	0.09	0.67	0.64	0.34	0.35	0.77	0.79
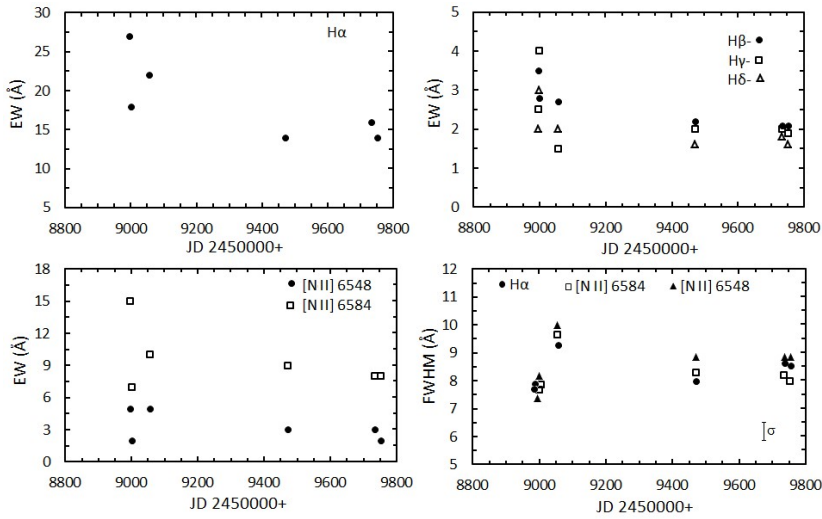
Fig. 6. Time variability of hydrogen lines EW – Hα (a), Hβ, Hγ, Hδ (b) and [NII] λ 6548, 6584 Å(c) lines. Panel (d) shows the variation of the FWHM of the Hα emission and the [NII] doublet λ 6548, 6584 Å. The vertical bar is the average error σ level.

years. In this case, the half-width of the $H\alpha$ line has the smallest value. This indicates that the equivalent widths are enhanced due to the line intensity, i.e., due to the additional radiation that appeared at that moment.

6. NEUTRAL HELIUM LINES

The spectrum of the star contains lines of neutral helium He I λ 4026, 4387, 4417, 4922, 6678 Å, etc. These lines are quite strong, which corresponds to the

spectrum of an early B star, and do not show any obvious traces of emission. Table 3 lists the measured equivalent widths of the strongest lines of He I. Since the expected spectral type of the star AS 310 should be B1- B2 (see Table 1), Table 3 shows that for the first three EW dates, most helium lines show anomalously large values for such a spectral type. This indicates that there may be a contribution from the spectrum of a nearby neighboring star in the helium lines. On the last 3 dates (Table 3), when the star shows a weakening of the emission in the $H\alpha$ and Hβ lines, relatively normal values of EW are observed. Table 3 also shows the average values of the equivalent widths over all observations, as well as the variance from the average over all data. To clarification of spectral type of the star AS 310, we used the equivalent width for 7 lines of He I given in Table 2. To do this, we compared our He I line equivalent widths with theoretical data for the same lines using the model of Auer and Michalas (1973). Figure 7 shows
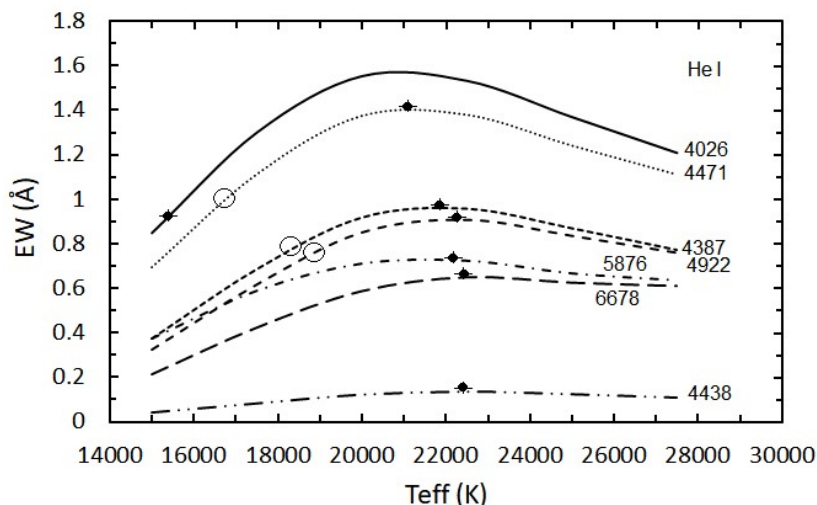

Fig. 7. Plot of the theoretical EW values of the He I lines versus temperature Teff at log g = 4.0 cgs, according to the model of Auer and Michalas (1973) for the normal chemical composition. The black circles show the EW values for our measurements in the active state of the emission spectrum, and the open circles show the values in the low state of the star's emission spectrum. Each line is marked with the corresponding wavelength of the spectral line.

a grid of theoretical equivalent widths for different effective temperatures at $\log g$ = 4.0 cgs with solar chemical composition. Each figured line corresponds to one helium spectral line. Black circles correspond to mean EW values. If these values exceeded the theoretical values, then the black dots were placed at the maximum of the theoretical EW curve. Open circles show the EW values corresponding to

the quiescent state of the emission spectrum of the star (the last three dates of observations). This case is singled out only for the He I $\lambda4471, 4387$, and 4922 lines. For the rest of the lines, the values of EW and the last three dates turned out to be greater than the theoretical values. We constructed a similar diagram for the case $\log g = 3.0$cgs, however, most of our EW values were found to be inconsistent with this plot. This unambiguously indicates that the star has a luminosity type close to V. In addition, the observed values of the equivalent widths on individual dates are about twice larger than the allowable contribution of one star. Comparison of the observational values of EW with the theoretical ones showed that rather, the spectrum of the star in terms of helium lines is combined, consisting of at least the spectrum of two stars. The temperature of one of them is about 22000 ± 500 K (according to the location of the black circles), and the temperature of the second star should be about 17000 ± 1000 K (according to the light circles) in Fig.7. Stars with such temperatures correspond to spectral types B1.5-2V and B 3-5V (see, for example, Pecaut&Mamajek, 2011). As can be seen from Table1, we get the same result, which is close to Brook's data. et al. (1993).

7. PHYSICAL PARAMETERS AND MODELLING

In addition to the gas-dust nebula in which AS 310 entered, the circumstellar environment of the star also complicated by the radiation of nearby stars in both the visible and the IR range. In addition to the second object, which is located at a distance of 3-4" from AS 310, and which was noted in the works of Bastian & Mundt (1979), Henning et al., (1994), several objects were found in the close environment of the star in the IR range. According to the 2MASS archive data (Skrutskie et al.2006), the star is located in the complex region HII, where up to 7 objects of AS 310 environment have been identified within a radius of 6.7". By using the 2MASS data (2003yCat.2246, 0C), presented in the database SIMBAD (VizieR), we have presented a list of all detected objects of AS 310 environment in Table 3. In columns of Table 3 for each object a distance in arcseconds from AS 310, type of objects, equatorial coordinates according to ICRS (2000), spectral types, and R-band magnitudes have been presented. Table 3. Identified objects in close environment of the AS 310 on the data 2MASS catalog. The strongest radiation from the close environment of the star belongs to the object with identification as NAME SH 2-61 2, which is fainter than AC310 at one magnitude in the R band. In addition, the IR object RMS G026.4488+01.7425A has the same coinciding coordinates as AS 310 itself. Therefore, we can assume that in spectrum AS 310, rather we are dealing with at least the radiation of the two nearest stars of the system.

Table 3. Identified objects in close environment of the AS 310 on the data 2MASS catalog.

No	Identifier	D (arcsec)	type	ICRS(2000) RA	ICRS(2000) DEC	Sp	MagR
1	EM * AS 310	0.00	Ae*	183321.194	-045805.976	B1e	12.62
2	RMS G026.4488+01.7425A	0.10	IR	183321.19	-045805.9		
3	PMN J1833-0458	2.88	Rad	183321.1	-045809		
4	NAME SH 2-61 2	4.35		183321.440	-045808.298	B1I	13.79
5	RMS G026.4488+01.7425B	4.58	HII	183321.21	-045801.4		
6	2MASS J18332120-0458013	4.87		183321.199	-045801.105		
7	NAME SH 2-61 Stellar Group	6.69	OpC	183321	-0458.2		

On the results of spectral observations, we can take the dominant spectral type of the system's brighter star as B2V (see also Table 1). For the B2V spectrum, the color indexes for normal MS stars are $(B - V)_Q = -0.21, (V - Rc)_0 = -0.094, (V - Ic)_0 = -0.23$ (Pecaut & Mamajek, 2013). According to Fig.2, the color indices B - V vary in the range from 1.0 to 1.9, $V - Rc$ - from -0.4 to 0.4 , and V - Ic from 0.2 to 0.9 . We obtained the maximum value of the amplitude of brightness changes in the V-band $\Delta V \sim 0.6$ mag, and the colors $\Delta (V - R_c) \sim 0.8$mag, $\Delta (B - V) \sim 0.9$ and $\Delta (V - I_c) \sim 0.6$ mag. The observed increase in the brightness of the system on different dates is apparently associated with an increase in the contribution of the second component of the system. With a more stable, minimum brightness state in the B and V bands (equal to 13.85 and 12.6, respectively (Fig. 1)), for the color-excess of the star B2V we obtain $E(B - V) = 1.21$, and for $Av = RE(B - V) = 3.75$ (here the standard reddening coefficient was taken as R = 3.1). Comparison with Table 1 showed that the obtained Av is in good agreement with the data Wichittanakom et al. 2012 (Av = 3.94), Brooke et al., 1993 (Av = 3.9). Then, assuming a more stable brightness state $V_0 = 12.6$ mag (Fig. 1), and the distance to the cluster is 2500pc, (Tabl.1) we can calculate the absolute magnitude for this value Av, as Mx = -3.14 mag. Taking into account the bolometric correction, we get Mvb = -5.20mag, and for the luminosity and radius of the primary star, $\log L/L\odot = 4.01$ and $R = 7.0 R\odot$, respectively. With this approach to the analysis of our data of observations, there remains an uncertainty in the parameters of the secondary component of the system. In addition, the accuracy of determining the parameters in this approach is due to the determination of the color indexes and, ultimately, the interstellar reddening coefficient, which, as is known, determined by poor accuracy.
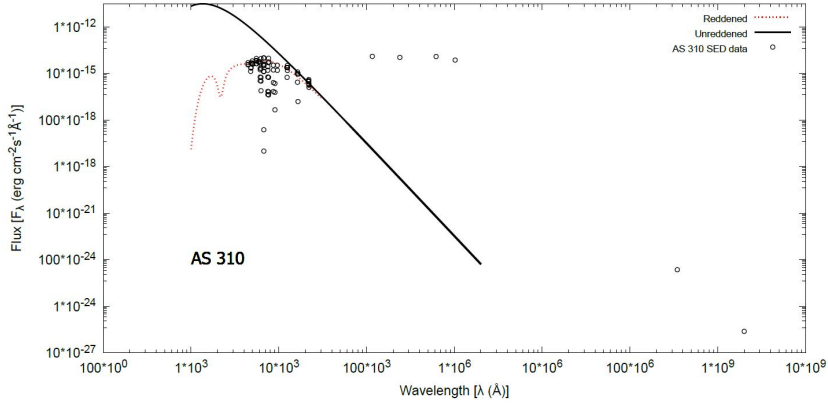
Fig. 8. SED data (empty circles) and model (solid and dotted curves) for AS 310. The observational SED data refers to within 2 arcsecs around the object.

Using the recently developed method proposed in the work by Bakis & Eker (2022), we considered the observational parameters of the binary system model for the AS 310 . The main point of this method is that a higher precision (~ 3 times) for the standard luminosities of stars could be obtained by using the multiband (Johnson B, V, Gaia G, GBp, GRp) bolometric corrections (BC) instead of using the Stefan-Boltzman law. Eker & Bak1s (2023) recently improved their method by including the BC for the Transiting Exoplanet Survey Satellite (TESS) passband.

To obtain the standard luminosities of binary star components, interstellar extinction in the abovementioned passbands and component light contributions of the binary system in the above-mentioned six passbands are needed which could be obtained by studying their spectral energy distribution (SED) data. The new method provides not only component contributions but also provides the amount of dimming due to interstellar extinction in magnitude scale $(A\xi)$ which is needed when computing absolute magnitude (M_ξ) of a component from its apparent magnitude ξ,

$$M_\xi = \xi + 5\log\pi + 5 - A\xi$$

where π and $A\xi$ are trigonometric parallax in arcseconds and interstellar extinction in magnitudes for the passband ξ, respectively. Together with the total magnitude of the binary star and its parallax, the equation of Bakis & Eker (2022) yields the absolute magnitudes of the components in the six passbands.

The interstellar extinction (A_ξ) of an object is a function of its unreddeed SED $\left(f_\lambda^0\right)$, its reddened SED (f_λ) and wavelength dependent filter sensitivity func-

tion $(S_\lambda(\xi))$ as follows:

$$A_\xi = 2.5 \log \frac{\int_0^\infty s_\lambda(\xi) f_\lambda^0(\text{ system })d\lambda}{\int_0^\infty s_\lambda(\xi) f_\lambda(\text{ system })d\lambda^2}$$

In this study, we retrieved the SED data of AS 310 using the SIMBAD database (Wenger et al. 2000) within an aperture of 2 ". Using the temperature of the components obtained above (T1=22000K and T2=17000 K) and the distance of 2500pc, the SED data is modelled. The radii of the components, which are not used in the calculation of standard luminosities but used for only obtaining interstellar extinction (A_g) in 6 passbands, are adopted from similar systems in the list of Double-Lined Detached Eclipsing Binaries (DDEBs) of Bakish & Eker (2022) as $R_1 = 4.0R_\odot$ and $R_2 = 2.6R_\odot$. After obtaining the standard luminosities, these radii are updated and listed in Table 4. In Fig. 8, the SED data is shown together with reddened and unreddened SED models. As it is seen in Fig. 8, the lower limit for the color excess is $E(B - V) = 1.0$ mag which denotes the multi-band interstellar extinctions as $A_B = 4.094$mag, $A_V = 3.066$mag, $A_G = 2.957$mag, $A_{GBp} = 3.526$mag, $A_{GRp} = 1.914$mag and $A_{TESs} = 1.980$mag. The SED data under the reddened model SED (dotted red curve in Fig. 8) imply higher extinctions are possible probably due to the state of the system. Therefore, it is expected to have different values of extinction depending on the observing time of the system, the case we have in this study.

The multiband BC s could be easily obtained by using the temperature-BC relations (see Table 2 of Eker & Bak1s, 2023 for all relation parameters) for each passband. Thus, the bolometric magnitude and the standard luminosities could be calculated using Eqs. 3 and 9, respectively. The methodology for determining parameter uncertainties is described for each parameter in Eker & Bakish (2023).

The multi-band absolute magnitudes $(M\xi)$, BCs, bolometric magnitudes $(Mbol\xi)$ and luminosity (L) of the components are given with their uncertainties in Table4. Using the Teff and L of the components, the radius for each component is calculated and presented in Table4 . As can be seen in Table 4 , the adopted radii of the components in the SED analysis are very close to the derived values.

Figure 9 shows the HR diagram with evolutionary tracks, taken from Vioque et al. (2022), where positions signed with black circles are well-known Herbig. AeBe stars (Ismailox et al..2022), the square and triangle marks the possible position of the main and secondary star of the system AS 310 . Hence, for the masses and the upper age limit, we obtain $M_1 = 9M_\odot, M_2 = 4.6M_\odot$ and $t < 1$Myr, accordingly.

8. DISCUSSION

The results of our photometric observations performed in 2016-2022 showed that the brightness and colors of AS 310 vary with time. Since the star is in a complex HII region and probably has similar stellar components nearby, this makes it difficult correctly distinguish the contribution of individual components of the system to the change in brightness and magnitude of the interstellar extinction coefficient in the direction of the system. We have shown that the seasonal
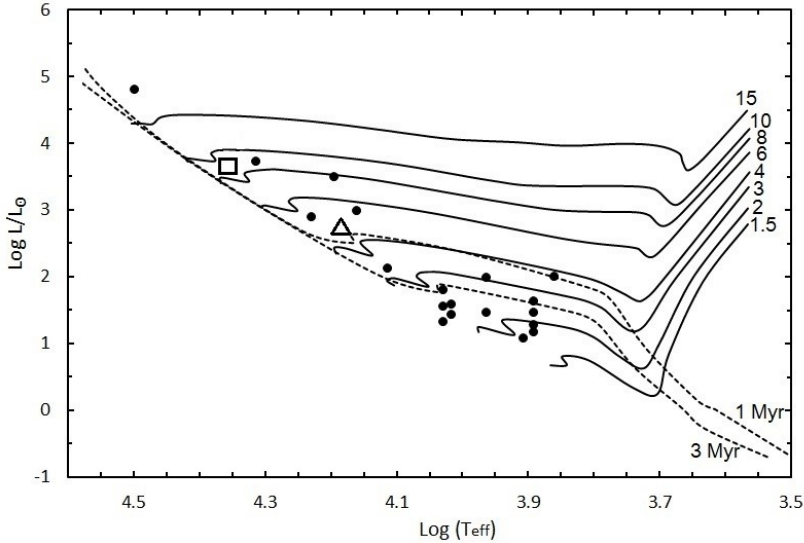

Fig. 9. HR diagram for well-known Herbig AeBe stars (black circles) Ismailov et al., 2022. Evolutionary tracks are plotted from data (Bressan et al. 2012 and Marigo et al. 2017). Bold lines indicate masses, dotted lines, –ages. The square and triangle marks the possible position of the main and secondary star of the system AS 310.

variations in the amplitude of the brightness in the V-band, starting from 2016, gradually increase and reach a maximum of 0.6 magnitudes in 2018. Then the amplitude of the brightness variations gradually decreases and reaches a minimum in 2022. On the branch of decreasing amplitude of the brightness variation in 2020-2022, we have executed spectral observations, which showed that in 2020 the emission spectrum in an enhanced state is observed. In 2021 and 2022, when the stellar brightness variability is minimal, the intensity of the emission has decreased significantly. In the quiescent state of the emission spectrum, the lines of neutral helium are comparable to the theoretical equivalent widths in the atmosphere of a star with spectra B1.5-2V and B3-5V. This result also confirms the assumption of the existence of a close companion of the star, which apparently contributes to the change in the brightness and spectrum of AS 310.

Table 4. Obtained parameters of separate components in binary system AS 310.

Parameter	Primary	Secondary
m_B (mag)	13.82 ± 0.01	15.338 ± 0.01
m_V (mag)	12.774 ± 0.01	14.221 ± 0.01
m_g (mag)	12.6458 ± 0.0028	14.0655 ± 0.0028
m_{GBp} (mag)	13.2827 ± 0.0028	14.7476 ± 0.0028
m_{GRp} (mag)	11.8437 ± 0.0028	13.2186 ± 0.0028
m_{TESS} (mag)	11.920 ± 0.014	13.294 ± 0.0028
BC_B (mag)	-1.789 ± 0.136	-1.190 ± 0.136
BC_V (mag)	-1.868 ± 0.12	-1.271 ± 0.12
BC_G (mag)	-1.926 ± 0.111	-1.323 ± 0.111
BC_{GBR} (mag)	-1.718 ± 0.127	-1.166 ± 0.127
BC_{GRR} (mag)	-2.188 ± 0.109	-1.510 ± 0.109
BC_{TESS} (mag)	-2.266 ± 0.111	-1.595 ± 0.111
M_B (mag)	-2.264 ± 0.093	-0.745 ± 0.093
M_V (mag)	-2.282 ± 0.093	-0.835 ± 0.093
M_G (mag)	-2.300 ± 0.093	-0.881 ± 0.093
M_{GBR} (mag)	-2.233 ± 0.093	-0.768 ± 0.093
M_{GRR} (mag)	-2.060 ± 0.093	-0.686 ± 0.093
M_{TESS} (mag)	-2.050 ± 0.094	-0.676 ± 0.094
$Mbol_B$ (mag)	-4.052 ± 0.164	-1.935 ± 0.164
$Mbol_V$ (mag)	-4.150 ± 0.151	-2.107 ± 0.151
$Mbol_G$ (mag)	-4.227 ± 0.144	-2.204 ± 0.144
$Mbol_{GBR}$ (mag)	-3.951 ± 0.157	-1.934 ± 0.157
$Mbol_{GRp}$ (mag)	-4.249 ± 0.143	-2.196 ± 0.143
$Mbol_{itess.}$ (mag)	-4.316 ± 0.145	-2.271 ± 0.145
Mbol	-4.168 ± 0.055	-2.119 ± 0.059
$L \, (L_\odot)$	3657 ± 187	555 ± 30
$R \, (R_\odot)$	4.16 ± 0.14	2.71 ± 0.11

The results of our observations can be qualitatively explained as follows: it is possible that when we observe anomalous EW values of helium lines, the contribution of the secondary component to the spectral lines increases. At the same time, an increase in the emission of hydrogen lines is observed, which may be the result of an increase in the emission of the nearby H II region due to an increase in the heating of the nebula by hot stars. The variability of emission in hydrogen lines, as well as their unusually small width for HAeBe stars, which was noted

also by Finkenzeller & Mundt (1984), confirms our conclusion that emission in hydrogen lines occurs in the H II region in the circumstellar gas under the UV radiation of the hot stars. The absence of emission components in the He I lines suggests that, rather, the stellar components of the system do not have the strong form of a circumstellar accretion disk. Similar hot OB stars have been detected before, for example, in the extremely young trapezium θ^1 Ori in the Orion Nebula M42 (see, for example, Parenago 1954, Antokhina et al. 1989, Balega et al. 2016). The observed brightness and spectrum variability in such massive systems is due to the dynamics of individual components in the system.

Thus, the revealed active and quiescent states of the stellar spectrum and brightness, the synchronous variation in the intensity of emission lines with the activity of changing brightness, and the anomalous values of the equivalent widths of helium lines in the active state can be explained in the model of the binary system. The observed variability may be the result of the visibility of the condition of radiation during the orbital motion of the components. Rather, it is an extremely young binary system, the components of which have reached the MS in about 1 Myr.

9. CONCLUSIONS

1. The star AS 310 is more often in a quiescent state of brightness, but from time to time, an increase in brightness with a variable amplitude is observed. The color and brightness of the star vary in different seasons. During the observation period 2016-2022, a smooth increase in the amplitude of the brightness variability in the V band have detected. Having reached a maximum in 2018 by 0.6 mag in the V band, the amplitude of brightness variations then gradually decreases to a minimum in 2022.

2. The same FWHM of the emission components have observed in the $H\alpha$, $H\beta$, and [NeII] lines, which indicates that these lines are formed in the HII region where the star is located, and the star itself does not have a significant protostellar disk. An increase in the emission in these lines is observed with an increase in the amplitude of variations in the brightness of the star.

3. Comparison of the equivalent widths with the theoretical spectrum for helium lines showed that the observed equivalent widths of neutral helium lines apparently refer to the combined spectrum of B3-5V and B1.5-2V. This showed that AS 310 is an extremely young binary system that quickly lost its circumstellar disk and entered the Main Sequence.

4. Using the method of spectral energy distribution of the star with the help of multicolor photometry, in model of the binary system the more probable phys-

ical parameters of the components and the evolutionary status of the system are determined.

REFERENCES

1. Abdullaev B.I., Alekberov I.A., Gyulmaliev N.I. et al., 2012 AzAJ, 7(4), 39*

2. Ageorges N., Eckart A., Monin J.-L., Menard F. 1997, A&A, **326**, 632*

3. Antokhina E.A., Ismailov N. Z., Cherepashchuk A.M., 1989, PAZh, **15**, 837*

4. Auer L.H., Mihalas D. 1973 ApJSS, **25**, 433*

5. Balega Yu.Yu., Chentsov E.L., Leushin V.V., et al., 2014, Astrophysical Bulletin, 69 (1), 46*

6. Bastian, U., Mundt , R. 1979, A&ASS, **36**, 57*

7. Bressan A., Marigo P., Girardi L., et al. 2012, MNRAS, **427**, 127*

8. Brooke T.Y., Tokunaga A.T., Strom S.E. 1993, AJ, **106**, 656.*

9. Bakış, V., Eker, Z. 2022, Acta Astronomica, 72, **3**, 195.*

10. Eker, Z., Bakış, V. 2023, MNRAS, 523, **2**, 2440.*

11. Finkenzeller U., Mundt R. 1984, A&ASS, **55**, 109*

12. Georgelin Y.P., Georgelin Y.M., 1970, A&A **6**, 349*

13. Gezer I., Ismailov N.Z, Mikailov Kh. M. et al., 2020 The Astronomer's Telegram No. 13992*

14. Goodrich R.W. 1993 ApJS **86**, 499*

15. Grankin KN, Melnikov S. Yu., Bouvier J., Herbst W., Shevchenko V.S. 2007 A&A **461**, 183*

16. Guzmán-Díaz J., Mendigutia I., Montesinos B.,et al., 2021 A&A, **650**, id.A182, 43 *

17. Henning Th., Launhardt E., Steinacker J., Thamm E., 1994, A&A **291**, 546*

18. Herbig G.H. 1960, ApJS , 4, 337*

19. Herbig G.H., Bell K.R. 1988, Lick Observatory Bulletin, 1111.*

20. Herbst W., Shevchenko V.S. 1999 AJ, **118**, 1043*

21. Hernandez J., Calvet N., Briceno C., Hartmann L. Berlind P. 2004 AJ , **127**.1682H*

22. Hunter D.A., Massey P. 1990, AJ, **99**, 846*

23. Ismailov N.Z., Alyshov S.A., Ismailova Sh.K., Huseynova F.S. 2023, Astron.Reports. (in press).*

24. Ismailov N.Z., Pogodin M. A., Bashirova, U. Z., Bahaddinova G. R. 2020a, Astron.Reports, 64, **1**, 23*

25. Ismailov N.Z., Mikhailov Kh.M., Khalilov O.V. et al. 2020 The Astronomer's Telegram No. 13861*

26. Ismailov N. .Z, Valiyev U. Z., Dzhalilov N. S., AzAJ 2022, Vol. **17**, No. 2, 40.*

27. Lahulla J.F. 1987 AJ, 94, 1062*

28. Lenz P., Breger M. 2005, CoAst , **146**, 53*

29. Lomb N.R. 1976, Ap&SS ,**39**, 447*

30. Manoj P., Bhatt H.C., Maheswar G., Muneer S. 2006, ApJ ,**653**, 657*

31. Marigo P., Girardi L., Bressan A., et al. 2017, ApJ , **835**, 77*

32. Parenago P.P. Trudy GAISH, MSU, 1954, XXV, 254-p.*

33. Pecaut M.J., Mamajek E.E. 2013, ApJSS 208, 9 (22pp)*

34. Pogodin M.A., Pavlovskij S.E., Drake N.A., et al., Stars: From Collapse to Collapse, Proceedings of a conference held at SAO, Nizhny Arkhyz , Russia 3-7 October 2016. Edited by Yu. Yu. Balega , D.O. Kudryavtsev , II Romanyuk , and I. A. Yakunin. San Francisco: ASP, 2017, p.157*

35. Ccargle J.D. 1982, ApJ , **263**, 835*

36. Skrutskie M.F., Cutri R.M., Stiening R., et al., 2006 AJ, **131**, 1163

37. Testi L., Palla F., and Natta A ., 1998 A&ASS., **133**, 81*

38. Valiyev U., Alishov S., Ismailov N.Z. 2022, Peremennye Zvezdy, 42 (9), 51*

39. Verhoeff A.P., Ababakr K.M., MNRAS 2020, **493**, 234*

40. Verhoeff A.P., Waters L.B.F.M.; van den Ancker M.E. et al., 2012A&A, **538**, 101*

41. Vioque M., Oudmaijer R.D., Schreiner M., et al., A&A, 2020, **638**, A21 *

42. Vioque M., Oudmaijer R.D., Wichittanakom Ch. et al. 2022, ApJ, **930**, 39*

43. Wichittanakom C., Oudmaijer R. D, Fairlamb J.R., Mendigut´ıa I ., et al., 2020 MNRAS **493**, 234*